



Top Quark Mass Measurement with the Matrix Element Method in the Lepton+Jets Final State at DØ Run II

The DØ Collaboration
URL <http://www-d0.fnal.gov>
(Dated: March 20, 2006)

We present a measurement of the top quark mass with the Matrix Element method in the lepton+jets final state. As the jet energy scale represents the dominant source of systematic uncertainty, the Matrix Element likelihood is extended by an additional parameter, which is defined as a global scale factor relative to the reference scale. The top quark mass is obtained from a fit which yields the combined statistical and systematic jet energy scale uncertainty. Using a data set of 370 pb^{-1} of data taken with the DØ experiment at Tevatron Run II, the mass of the top quark is measured to be

$$m_{\text{top}}^{\ell+\text{jets}}(\text{topo}) = 169.2_{-7.4}^{+5.0} (\text{stat.} + \text{JES})_{-1.4}^{+1.5} (\text{syst.}) \text{ GeV} \text{ and}$$
$$m_{\text{top}}^{\ell+\text{jets}}(b\text{-tag}) = 170.6_{-4.7}^{+4.0} (\text{stat.} + \text{JES}) \pm 1.4 (\text{syst.}) \text{ GeV} ,$$

where information about identified b jets is only used in the second result. The measurements yield a jet energy scale consistent with the reference scale.

Preliminary Results for Moriond 2006

I. INTRODUCTION

The matrix element method has been used previously by DØ at Tevatron Run II [1] to measure the top quark mass in $t\bar{t}$ events. In this note, an update of this measurement is presented. The method has been extended to include information from b tagging, and results are presented both for an analysis that makes use of this additional information and for the previous method, which uses topological information only. In addition, the data sample analyzed has been extended to 370 pb^{-1} .

In $p\bar{p}$ collisions at $\sqrt{s} = 1.96 \text{ TeV}$, top quarks are predicted in the Standard Model to be produced dominantly as top-antitop pairs via $q\bar{q}$ annihilation (85%) and gluon fusion (15%). Both top and antitop are predicted to decay almost exclusively to a W boson and a b quark. If one of the W bosons decays hadronically to a pair of light quarks, while the other decays to either an electron or muon and the corresponding neutrino, the event is referred to as a *lepton+jets* (ℓ +jets) event. The signature of this decay in the detector is the presence of four or more jets, two of which come from a b quark, an isolated lepton, and missing transverse energy \cancel{E}_T from the undetected neutrino. The dominant physics background to this process is the electroweak production of a leptonically decaying W in association with four or more quarks and gluons. Additional instrumental background arises from multi-jet events, where either a heavy flavor jet decays semi-leptonically but only the muon is reconstructed (μ +jets channel) or a jet is misidentified as an electron (e +jets channel). This instrumental background is referred to as “QCD” background throughout this note and is expected to be small and of similar topology as $W(\rightarrow l\nu) + \text{jets}$.

II. THE DØ DETECTOR

The DØ detector has a central-tracking system, consisting of a silicon microstrip tracker (SMT) and a central fiber tracker (CFT), both located within a 2 T superconducting solenoidal magnet [2], with designs optimized for tracking and vertexing at pseudorapidities $|\eta| < 3$ and $|\eta| < 1.6$, respectively. A liquid-argon and uranium calorimeter has a central section (CC) covering pseudorapidities $|\eta|$ up to ≈ 1.1 , and two end calorimeters (EC) that extend coverage to $|\eta| \approx 4.2$, with all three housed in separate cryostats [3]. An outer muon system, at $|\eta| < 2$, consists of a layer of tracking detectors and scintillation trigger counters in front of 1.8 T toroids, followed by two similar layers after the toroids [4].

Trigger and data acquisition systems are designed to accommodate the luminosities of Run II. Based on preliminary information from tracking, calorimetry, and muon systems, the output of the first level of the trigger is used to limit the rate for accepted events to $\approx 2 \text{ kHz}$. At the next trigger stage, with more refined information, the rate is reduced further to $\approx 1 \text{ kHz}$. The third and final level of the trigger, with access to all the event information, reduces the output rate to $\approx 50 \text{ Hz}$, which is written to tape.

III. EVENT SELECTION

The event selection is identical to that used in [1]. It has been mainly adopted from the topological top quark cross section analyses in the e +jets and μ +jets channels at DØ for Run II [5]. Events are selected requiring an isolated energetic charged lepton ($p_T > 20 \text{ GeV}$, electron: $|\eta| < 1.1$; muon: $|\eta| < 2$), significant missing transverse energy ($\cancel{E}_T > 20 \text{ GeV}$), and exactly four good calorimeter jets ($p_T > 20 \text{ GeV}$, $|\eta| < 2.5$). A $\Delta\phi$ cut between the lepton and \cancel{E}_T is imposed to reject events in which the transverse energy imbalance originates from a poor lepton energy measurement. The official certified DØ jet energy corrections including η dependent corrections are applied to the jets in the event. All jet energy corrections are propagated to \cancel{E}_T before the selection of the sample.

This selection yields 86 and 89 events for the 370 pb^{-1} DØ Run II data sample in the e +jets and μ +jets channel respectively. The same topological likelihood technique used in [1] is used to obtain estimates on the signal fraction as well as the contribution from instrumental background (QCD) in the sample. The fits are shown in Figure 1, and the results are summarized in Table I.

A $t\bar{t}$ event contains two b jets, while jets produced in association with W bosons predominantly originate from light quarks or gluons. That is why the signal to background ratio is significantly enhanced after the requirement that at least one of the jets is b tagged. DØ developed a lifetime based b tagging algorithm referred to as SVT [6] which is used in the b tagging analysis to identify jets consistent with originating from a b quark.

The performance of the SVT algorithm is extensively tested on data. The b tagging efficiency is verified on a dijet data sample whose b jet content is enhanced by requiring that one of the jets be associated with a muon. The distribution of the transverse momentum of the muon relative to the associated jet axis is used to extract the fraction of b jets before and after tagging. The probability to tag a light quark jet (mistag rate) is inferred from the rate of secondary vertices with negative impact parameter, corrected for the contribution of the heavy flavor jets to such tags

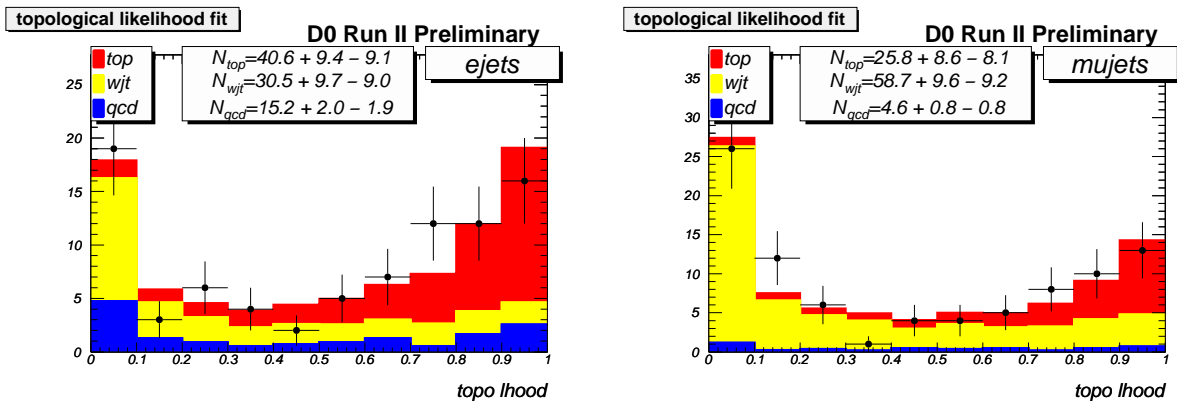


FIG. 1: Topological likelihood fit applied to the 370 pb^{-1} DØ Run II data sample. The topological likelihood for e +jets events is shown in the left plot, that for μ +jets events in right plot. The points with error bars indicate the data, and the fitted fractions of $t\bar{t}$ events (red), W +jets events (yellow), and QCD multijet events (blue) are superimposed. The technique is identical to that used in [1].

channel	N_{evts}	$f_{\text{top}}^{\text{topo}}$	$N_{\text{top}}^{\text{topo}}$	$f_{\text{QCD}}^{\text{topo}}$
e +jets	86	$47.2^{+10.9}_{-10.6} \%$	$40.6^{+9.4}_{-9.1}$	$17.6^{+2.4}_{-2.2} \%$
μ +jets	89	$29.0^{+9.7}_{-9.1} \%$	$25.8^{+8.6}_{-8.1}$	$5.1^{+0.9}_{-0.8} \%$
ℓ +jets	175	$37.9^{+7.3}_{-7.0} \%$	$66.4^{+12.7}_{-12.2}$	$11.3 \pm 1.2 \%$

TABLE I: Composition of the e +jets, μ +jets, and ℓ +jets data samples, estimated with the topological likelihood technique.

and the presence of long lived particles in light quark jets. Both corrections are derived from Monte Carlo simulation. Both the b jet tagging efficiency $\epsilon_{\text{jet}}(b)$ and the light jet tagging rate $\epsilon_{\text{jet}}(u, d, s)$ are parameterized as functions of the transverse jet energy and pseudorapidity. The efficiency $\epsilon_{\text{jet}}(c)$ to tag a c quark jet is estimated based on the Monte Carlo prediction for the b to c jet tagging efficiency ratio. These parameterizations are used to predict the probability for a jet of a certain flavor to be tagged.

IV. TOPOLOGICAL ANALYSIS

A. Method

The topological analysis uses the same method that is described in [1]; the fitting technique for the top quark mass and jet energy scale has however been extended to allow for asymmetric errors. The probability of any event to be produced via a certain process is proportional to the differential cross section of that process. Consequently, the probabilities P_{sgn} and P_{bkg} for events to originate from the $t\bar{t}$ signal and the W +jets background process are calculated based on the respective matrix elements $\mathcal{M}_{t\bar{t}}$ and $\mathcal{M}_{W+\text{jets}}$. The leading order matrix element is taken for $q\bar{q} \rightarrow t\bar{t}$ production, and W +jets events are described with the VECBOS [7] parameterization of the matrix element. The energy resolutions for muons and jets are taken into account as well. Transfer functions $W(E_j, E_p)$ are derived from Monte Carlo, which describe the probability for a parton with energy E_p to be reconstructed with E_j in the detector. Jet and lepton angles and electron energies are assumed to be well measured, and the probabilities are obtained by integrating over all possible parton states, where each state is weighted by its probability to produce the observed measurement. The transverse momentum of the neutrino is obtained from the p_T imbalance of the five detected final state objects. All jet permutations and neutrino solutions are considered with equal a priori weight.

The signal probability is normalized by computing the integral of P_{sgn} over the 16-dimensional parton phase space as a function of m_{top} and JES , as described in [1]. The background probability P_{bkg} is calibrated such that the fitted signal fraction f_{top} yields the true $t\bar{t}$ fraction in Monte Carlo ensemble tests on average for all top quark mass samples.

For the topological analysis, the total event probability is defined as in [1] by combining both probabilities according to

$$P_{\text{evt}}(x; m_{\text{top}}, JES, f_{\text{top}}) = f_{\text{top}} \cdot P_{\text{sgn}}(x; m_{\text{top}}, JES) + (1 - f_{\text{top}}) \cdot P_{\text{bkg}}(x; JES) , \quad (1)$$

where x denotes all kinematic variables of the reconstructed lepton and jets. f_{top} is the signal fraction in the sample under study. The signal probability is sensitive to the jet energy scale parameter JES , because the mass of the hadronically decaying W boson is constrained in the $t\bar{t}$ matrix element. It has been found that it is sufficient to calculate the background probability only for one JES hypothesis, i.e. $P_{\text{bkg}}(x; JES) = P_{\text{bkg}}(x; 1.0)$.

In order to extract the top quark mass from a set of N events with measurements x_1, \dots, x_N , a likelihood function is built from the event probabilities,

$$L(x_1, \dots, x_N; m_{\text{top}}, JES, f_{\text{top}}) = \prod_{i=1}^N P_{\text{evt}}(x_i; m_{\text{top}}, JES, f_{\text{top}}) , \quad (2)$$

and evaluated for different hypotheses of m_{top} and JES . For every (m_{top}, JES) hypothesis, the likelihood is maximized with respect to f_{top} to obtain a two-dimensional grid of likelihood values.

For each top quark mass hypothesis, the likelihood values as a function of assumed JES value are integrated to obtain the likelihood value for this top quark mass. This yields a graph of likelihood values as a function of top quark mass, from which the top quark mass measurement is extracted. The $-\ln L$ values are fitted with a fourth order polynomial in the region $\Delta \ln L < 3$ around the best value. The measured top quark mass is the value of m_{top} where this function has its minimum, and an asymmetric 68% confidence level interval around this central value is obtained from the graph of likelihood values. The corresponding procedure is used to obtain the measurement of the jet energy scale JES .

B. Calibration of the Topological Analysis

The same Monte Carlo ensemble testing procedure that is described in [1] is also used for the calibration of the new fitting method. The calibration curves are very similar, indicating consistency between the previous and new fitting techniques.

The calibration derived for the ℓ +jets sample is shown in Figure 2. The pull width for both m_{top} and JES is in good agreement with 1.0, indicating a trustworthy error estimate by the likelihood procedure. Figure 3 illustrates that the fitted top mass does not depend on the true jet energy scale in the sample. The calibrations of both parameters are applied to the result obtained from the data sample.

C. Result of the Topological Analysis

The matrix element method is applied to the 370 pb^{-1} ℓ +jets data set collected at $D\bar{O}$ during Run II. The calibrations for m_{top} derived in the previous section are taken into account. The statistical uncertainty yielded by the mass fit is inflated according to the deviations of the pull width from 1.0. The calibrated fit result for the combined ℓ +jets sample is shown in Figure 4. The top mass is measured to be

$$m_{\text{top}}^{\ell+\text{jets}} = 169.2_{-7.4}^{+5.0} (\text{stat.} + \text{JES}) \text{ GeV} .$$

A comparison with the expected errors is given in Figure 5. For a fixed jet energy scale, the statistical error of the fit is $_{-3.5}^{+3.7}$ GeV; thus the component from the jet energy scale uncertainty is $_{-6.5}^{+3.4}$ GeV.

The fitted jet energy scale of $1.048_{-0.040}^{+0.052} (\text{stat.})$ indicates that the scale in the simulation is consistent with that in the data.

V. ANALYSIS USING B TAGGING INFORMATION

A. Method

In the second analysis, b tagging information enters in two ways. The event sample is split into three subsamples of different $t\bar{t}$ purity according to how many jets were b tagged, and b tagging information is used to improve the selection of the correct jet-parton assignment.

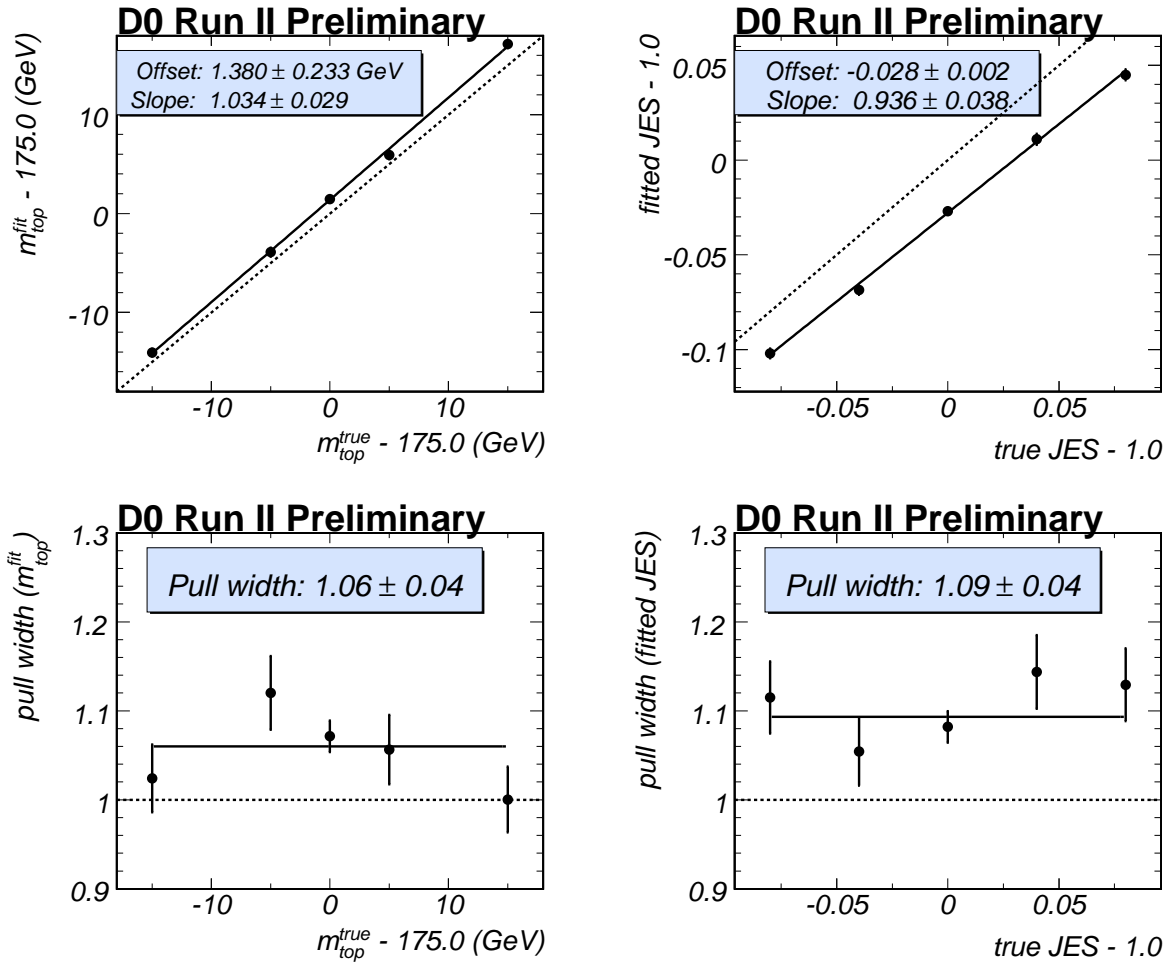


FIG. 2: Calibration of the matrix element mass fitting procedure for the topological analysis. The upper plots show the reconstructed top mass as a function of input top mass (upper left) and the measured jet energy scale as a function of input scale (upper right). Also shown are the results of linear fits to the points, which are used to calibrate the measurement technique. The two lower plots show the widths of the pull distributions for the top mass (lower left) and jet energy scale (lower right), together with the weighted means of the pull widths. The dashed lines in the upper plots indicate offset 0 and slope 1, in the lower plots they indicate a pull width of 1.

The three subsamples used in the b tagging analysis are exclusive and correspond to 1) no b tagged jet, 2) exactly 1 tagged jet, and 3) two or more tagged jets. The relative contributions from background events with a W boson and four jets with different flavor composition are estimated using the Alpgen [8] generator. The fractions f_{Φ} of each of the six flavor configurations $\Phi = jjjj, b\bar{b}jj, c\bar{c}jj, (b\bar{b})jjj, (c\bar{c})jjj,$ and $cjjj$ (the symbols $(b\bar{b})$ and $(c\bar{c})$ refer to situations where two heavy flavor quarks end up in the same jet) are listed in Table II [6]. These fractions are obtained without a b tagging requirement; they are significantly changed in each of the three separate classes of events.

The jets in selected QCD multijet background events have kinematic characteristics similar to those of jets in selected W +jets background events. Concerning the event b tagging probabilities, we therefore do not distinguish between QCD multijet and W +jets backgrounds. The difference between multijet and W +jets kinematics is treated as a systematic uncertainty.

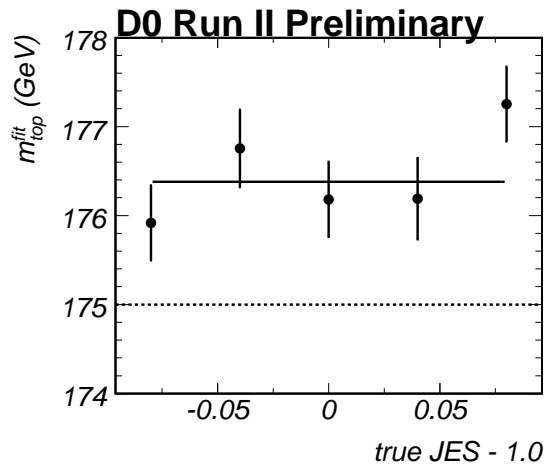


FIG. 3: Fitted top mass for the topological analysis as a function of true jet energy scale JES and for a true top mass of 175 GeV: the reconstructed top mass does not depend on the input jet energy scale. Also shown is the value of the calibration curve as obtained from Figure 2 for 175 GeV top mass.

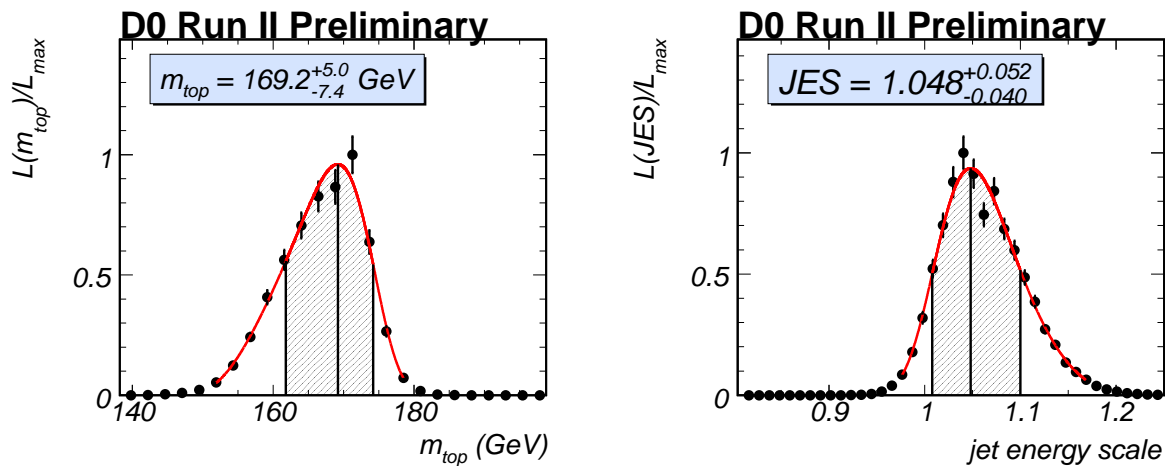


FIG. 4: Application of the topological analysis to the $370 \text{ pb}^{-1} \ell + \text{jets}$ data set. The m_{top} and JES axes correspond to the calibrated values. The left plot shows the likelihood as a function of m_{top} hypothesis, together with the result of the fourth order polynomial fit to the corresponding $-\ln L$ graph. Also shown are the fitted central value and the 68% confidence level interval. The same information is provided in the right plot for the determination of the JES parameter.

Contribution	$W + \geq 4 \text{ jets}$
$Wbbjj$	$(2.72 \pm 0.11) \%$
$Wc\bar{c}jj$	$(4.31 \pm 0.20) \%$
$W(b\bar{b})jjj$	$(2.70 \pm 0.15) \%$
$W(c\bar{c})jjj$	$(4.69 \pm 0.36) \%$
$Wcjjj$	$(4.88 \pm 0.17) \%$
$W + \text{light jets}$	$(80.71 \pm 0.43) \%$

TABLE II: Fractions f_{Φ} of different flavor subprocesses contributing to the $W + \text{jets}$ sample.

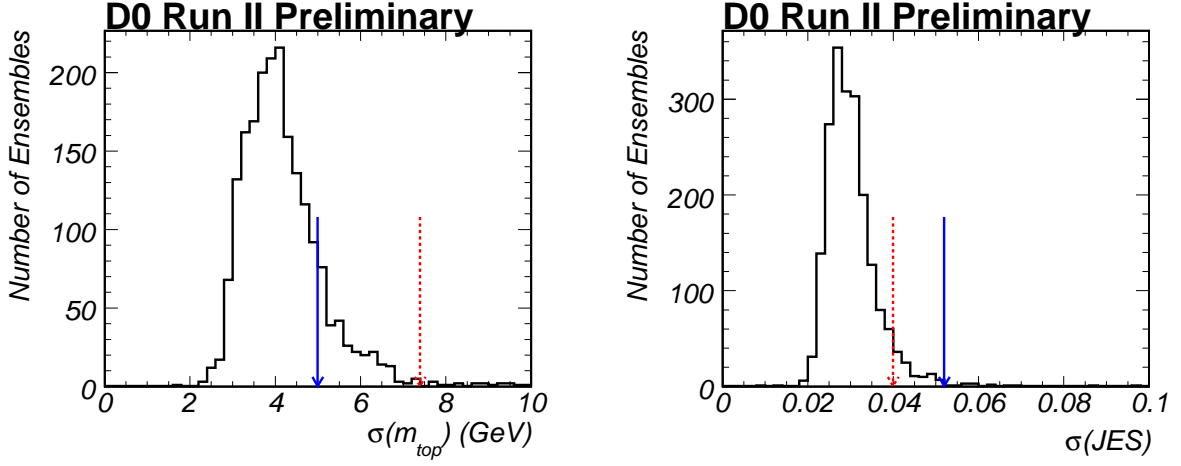


FIG. 5: Errors on m_{top} (left) and JES (right) obtained with the topological analysis. The distributions of fitted uncertainties obtained from ensemble tests are shown by the histograms. Both upper and lower uncertainties are shown; their distributions are very similar. The upper (lower) error in the data is indicated by the solid blue (dashed red) arrow. The probability for a lower error on m_{top} with a magnitude larger than that observed in the data is 2%.

The efficiencies to tag exactly 0, 1, and ≥ 2 jets in a given event with four reconstructed jets are determined by

$$\begin{aligned}
 \epsilon^0 &= \prod_{j=1}^4 (1 - \epsilon_{\text{jet}}(\alpha_k; E_j^{\text{T}}, \eta_j)) , \\
 \epsilon^1 &= \sum_{j_{\text{tag}}=1}^4 \epsilon_{\text{jet}}(\alpha_k; E_{j_{\text{tag}}}^{\text{T}}, \eta_{j_{\text{tag}}}) \prod_{j=1; j \neq j_{\text{tag}}}^{N_{\text{jets}}} (1 - \epsilon_{\text{jet}}(\alpha_k; E_j^{\text{T}}, \eta_j)) , \text{ and} \\
 \epsilon^{\geq 2} &= 1 - \epsilon^0 - \epsilon^1 ,
 \end{aligned} \tag{3}$$

where α_k is the flavor (b , c , light) of the parton in the direction of the corresponding jet. The per jet tagging efficiencies ϵ_{jet} depend on the jet transverse energy E_j^{T} and pseudorapidity η_j . Jets of any flavor can be tagged by the SVT algorithm, although the probability is highest for b jets. In the analysis, all possible jet flavor permutations $\{\alpha_i\}$ are considered. Therefore, the signal and background event tagging efficiencies are defined as

$$\begin{aligned}
 \epsilon_{\text{sgn}}^{n_{\text{tag}}} &= \frac{1}{2} \left(\epsilon_{t\bar{t}}^{n_{\text{tag}}}(\{\alpha_i\} = bbud) + \epsilon_{t\bar{t}}^{n_{\text{tag}}}(\{\alpha_i\} = bbcs) \right) \text{ and} \\
 \epsilon_{\text{bkg}}^{n_{\text{tag}}} &= \sum_{\Phi} f_{\Phi} \epsilon_{\Phi}^{n_{\text{tag}}} .
 \end{aligned} \tag{4}$$

These efficiencies are then used to relate the purities of the three tag categories to the inclusive signal purity f_{top} . The purity of the n_{tag} sample is given by

$$f_{\text{top}}^{n_{\text{tag}}} = \frac{N_{\text{sgn}}^{n_{\text{tag}}}}{N_{\text{sgn}}^{n_{\text{tag}}} + N_{\text{bkg}}^{n_{\text{tag}}}} \tag{5}$$

and can be expressed as a function of the inclusive signal purity (f_{top}) as

$$f_{\text{top}}^{n_{\text{tag}}} = \frac{f_{\text{top}} r^{n_{\text{tag}}}}{f_{\text{top}}(r^{n_{\text{tag}}} - 1) + 1} \tag{6}$$

where

$$r^{n_{\text{tag}}} = \frac{\epsilon_{\text{sgn}}^{n_{\text{tag}}}}{\epsilon_{\text{bkg}}^{n_{\text{tag}}}} . \tag{7}$$

In addition to dividing the sample into three categories, b tagging information is used to weight different jet-parton assignments. The optimal weight for a permutation i is given by

$$w_i = \prod_{\text{tagged jets } j} \epsilon_{\text{jet}}(\alpha_k; E_j^T, \eta_j) \prod_{\text{untagged jets } j} (1 - \epsilon_{\text{jet}}(\alpha_k; E_j^T, \eta_j)) , \quad (8)$$

where α_k denotes the flavor of the parton k in the direction of the corresponding tagged or untagged jet j with transverse energy E_j^T and pseudorapidity η_j . For events without a b tagged jet, this leads to each permutation being assigned an equal weight of $w_i = 1/24$ as in the topological analysis.

To compute the signal probability of events containing b tagged jets, Equation (8) is slightly simplified to reduce the computation time: If an event contains exactly one b tagged jet, the quarks from the hadronic W decay are both assumed to be light quarks (u , d , or s). This is justified since the tagging efficiencies for b jets are much larger than those for other flavors, and there are two b jets per event. For events with two or more b tagged jets, a charm jet from the hadronic W decay is tagged in a non-negligible fraction of cases. Consequently, the quarks from the hadronic W decay are assumed to be charm quarks if the corresponding jet has been tagged, and light quarks otherwise.

Because the different flavor contributions to the W +jets process are described by the same matrix element, and that matrix element describes a process without heavy quarks in the final state, the weights w_i for the background probability are all equal even if b tagged jets are present. Therefore, the background probability calculated for the topological analysis can be used in the b tagging analysis without modifications.

Event likelihoods are built as a function of m_{top} and JES hypotheses for each of the three classes of events as

$$P_{\text{evt}}^{n_{\text{tag}}}(x; m_{\text{top}}, JES, f_{\text{top}}) = f_{\text{top}}^{n_{\text{tag}}} \cdot P_{\text{sgn}}^{n_{\text{tag}}}(x; m_{\text{top}}, JES) + (1 - f_{\text{top}}^{n_{\text{tag}}}) \cdot P_{\text{bkg}}(x; JES) , \quad (9)$$

where $P_{\text{evt}}^{n_{\text{tag}}}$ is the signal probability calculated according to the weight w_i defined above, and P_{bkg} is computed identically to the topological analysis. In order to extract the top quark mass from the total sample of selected events, these likelihoods are combined as

$$L(x_1, \dots, x_N; m_{\text{top}}, JES, f_{\text{top}}) = \prod_{n_{\text{tag}}=0,1,\geq 2} \prod_{i=1}^{N^{n_{\text{tag}}}} P_{\text{evt}}^{n_{\text{tag}}}(x_i; m_{\text{top}}, JES, f_{\text{top}}) , \quad (10)$$

where $N^{n_{\text{tag}}}$ is the number of events in each of the three tag categories. The symbol f_{top} denotes one parameter that describes the fraction of $t\bar{t}$ events in the total event sample, as in the topological analysis. The signal fractions $f_{\text{top}}^{n_{\text{tag}}}$ in each of the three event classes are computed from this overall signal fraction f_{top} and the event tagging efficiencies according to Equations (6) and (7).

The top quark mass and jet energy scale are then obtained by the same fitting technique as used in the topological analysis.

The calibration, using the procedure of Section IV, is presented in Figures 6 and 7.

B. Result of the B Tagging Analysis

The Matrix Element b tagging method is applied to the same event sample as in Section IV with an identical calibration procedure according to numbers shown in Figure 6. The two-dimensional likelihood of the fitted m_{top} and JES values from data for the corresponding best value for f_{top} is projected against the corresponding axis and plotted in Figure 8 for each of the three tag categories. The result for the combined event sample is

$$m_{\text{top}}^{\ell+\text{jets}} = 170.6_{-4.7}^{+4.0} (\text{stat.} + \text{JES}) \text{ GeV} \quad (11)$$

and is shown in Figure 9. The 68% confidence level intervals around the mean are indicated under the fitted curve. Figure 10 shows the distributions of the expected negative and positive m_{top} and JES uncertainties compared to the observed result.

VI. SYSTEMATIC UNCERTAINTIES

Systematic uncertainty arise from three sources: modeling of the physics processes for $t\bar{t}$ production and background, modeling of the detector performance, and uncertainties in the methods themselves. Table III lists all uncertainties.

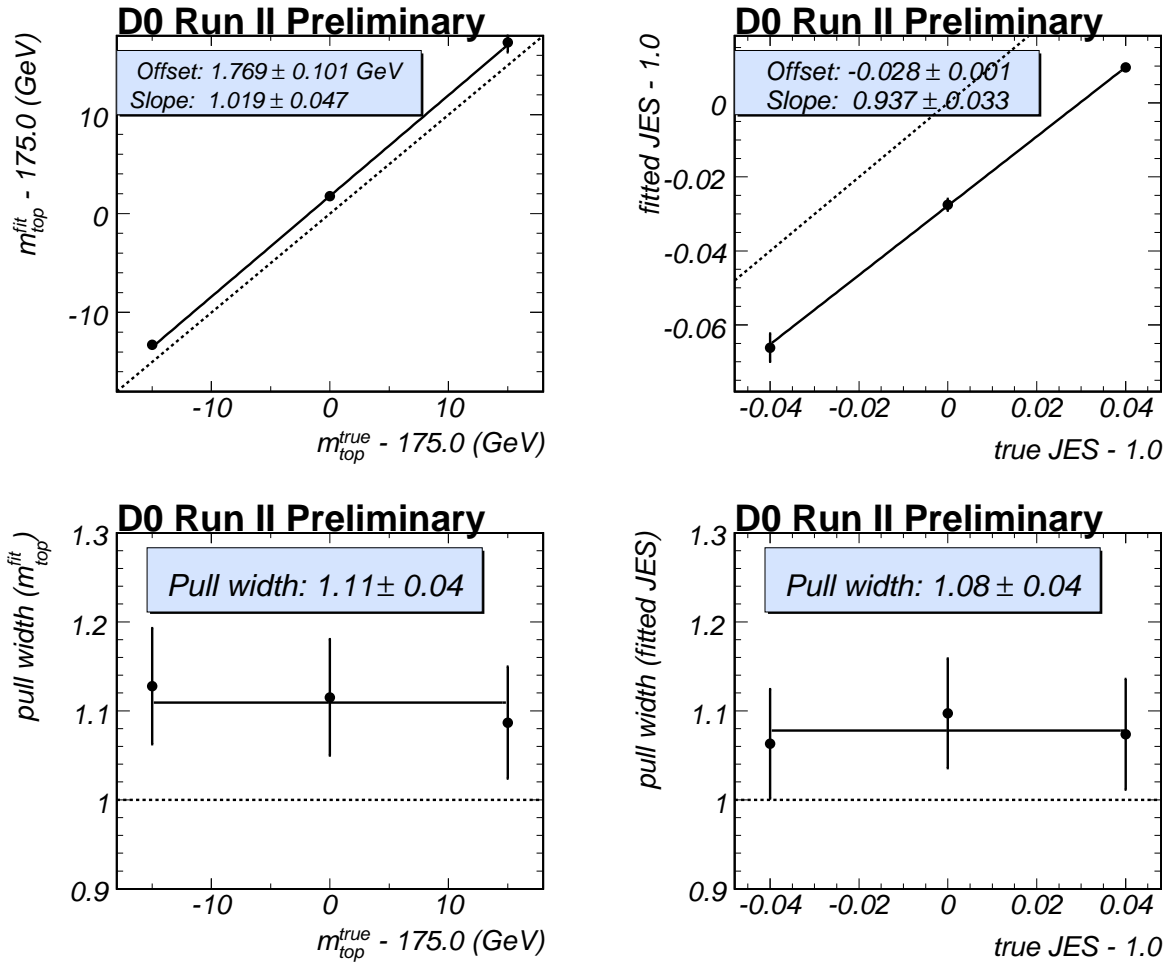


FIG. 6: Calibration of the matrix element mass fitting procedure for the b tagging analysis. The upper plots show the reconstructed top mass as a function of input top mass (upper left) and the measured jet energy scale as a function of input scale (upper right). Also shown are the results of linear fits to the points, which are used to calibrate the measurement technique. The two lower plots show the widths of the pull distributions for the top mass (lower left) and jet energy scale (lower right), together with the weighted means of the pull widths. The dashed lines in the upper plots indicate offset 0 and slope 1, in the lower plots they indicate a pull width of 1.

The jet energy scale uncertainty is included in the statistical error. The total systematic uncertainty on the top mass measurement is obtained by adding all contributions in quadrature. In general, to evaluate systematic uncertainties, the simulation of events used to calibrate the measurement has been varied, while the measurement method itself has been kept unchanged. In a number of cases, no large difference is expected between the uncertainties for the two analyses, and the uncertainty from the topological analysis is assigned for both measurements.

A. Physics Modeling

- **Signal modeling:** When $t\bar{t}$ events are produced in association with a jet, the additional jet can be misinterpreted as a product of the $t\bar{t}$ decay. Also, the $t\bar{t}$ system may then have significant transverse momentum, in contrast to the assumption made in the calculation of P_{sgn} . In spite of the event selection that requires exactly four jets, these events can be selected if one of the jets from the $t\bar{t}$ decay is not reconstructed.

Such events are present in the simulated events used for the calibration of the method. To assess the uncertainty in the modeling of these effects, events have been generated using a dedicated $t\bar{t}$ +jets simulation. The fraction of such events simulated with extra jets is estimated to be no larger than 30% (according to the difference between

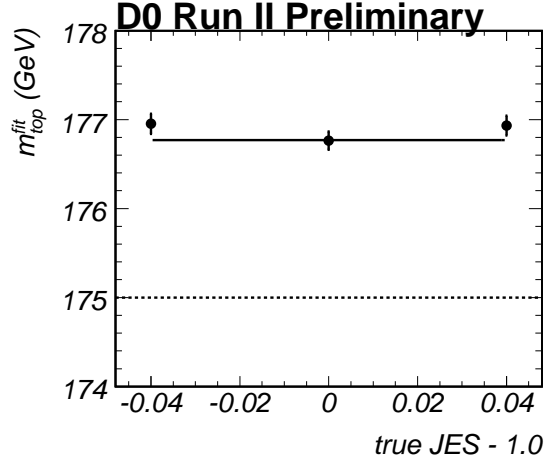


FIG. 7: Fitted top mass for the b tagging analysis as a function of true jet energy scale JES and for a true top mass of 175 GeV: the reconstructed top mass does not depend on the input jet energy scale. Also shown is the value of the calibration curve as obtained from Figure 6 for 175 GeV top mass.

Error Source	Topological Analysis	b Tagging Analysis
statistical error and jet energy scale	+5.0 - 7.4	+4.0 - 4.7
<i>physics modeling:</i>		
signal modeling	± 0.34	± 0.46
background modeling	± 0.32	± 0.32
PDF uncertainty	+0.35 - 0.20	± 0.07
b fragmentation	± 0.71	± 0.71
b/c semileptonic decays	+0.06 - 0.07	+0.06 - 0.07
<i>detector modeling:</i>		
JES p_T dependence	± 0.25	± 0.25
b response (h/e)	+0.87 - 0.75	+0.87 - 0.75
trigger	± 0.08	± 0.08
b tagging	-	± 0.24
<i>method:</i>		
signal fraction	+0.50 - 0.17	± 0.15
QCD contamination	± 0.67	± 0.29
MC calibration	± 0.17	± 0.48
total systematic error	+1.5 - 1.4	± 1.4
total error	+5.2 - 7.5	+4.2 - 4.9

TABLE III: Summary of uncertainties on the top quark mass. All errors are quoted in GeV.

cross-section calculations in leading and next-to-leading order).

Two large ensembles of simulated events are composed according to the sample composition in the data, one using only $t\bar{t}$ +jets events for the signal, and the second with the default simulation. The result obtained with the default simulation is quoted as central value. A systematic error of 30% of the difference in top mass results between these two ensembles is quoted.

In addition, simulated $gg \rightarrow t\bar{t}$ and $q\bar{q} \rightarrow t\bar{t}$ events have been compared. The top mass calibration has been

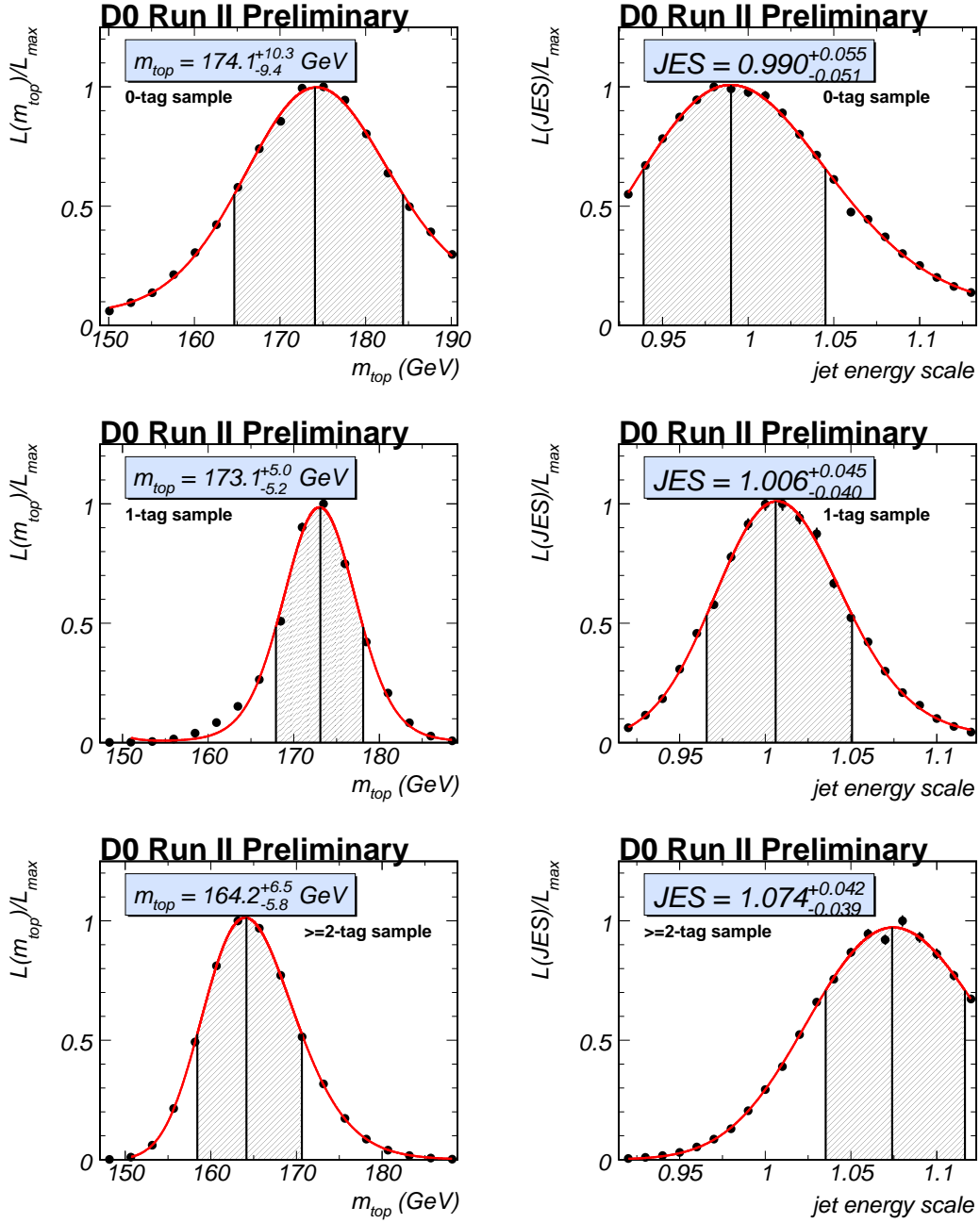


FIG. 8: Application of the Matrix Element b -tagging method to the data. The fitted m_{top} and JES likelihoods for each of the 3 tag categories: The two upper plots show the results in the 0-tag sample, followed by the results in the 1-tag sample, and the two lower plots show the results obtained in the ≥ 2 -tag sample. The 68% confidence-level interval around mean is indicated under each fitted curve.

rederived using only $gg \rightarrow t\bar{t}$ or $q\bar{q} \rightarrow t\bar{t}$ events to simulate the signal, and no significant difference has been found. Thus no additional uncertainty on the result is assigned.

- **Background modeling:** In order to study the sensitivity of the measurement to the choice of background model, the standard W +jets Monte Carlo sample is replaced by an alternative sample with the default factorization scale of $Q^2 = m_W^2 + \sum_j p_{T,j}^2$ replaced by $Q^2 = \langle p_{T,j} \rangle^2$. One large ensemble of events is composed using both the default and the alternative background model. The difference of results obtained with these ensembles is symmetrized and is assigned as systematic uncertainty.

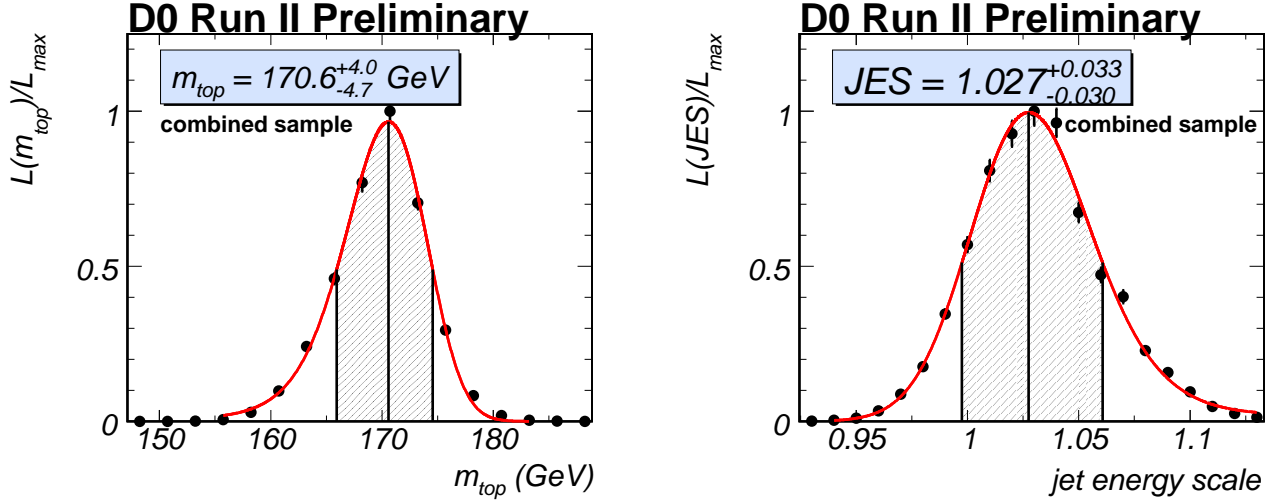


FIG. 9: Application of the Matrix Element b -tagging method to the data. The final result on the fitted m_{top} (left) and JES (right) likelihoods for the combined event sample. The 68% confidence-level interval around mean is indicated as well.

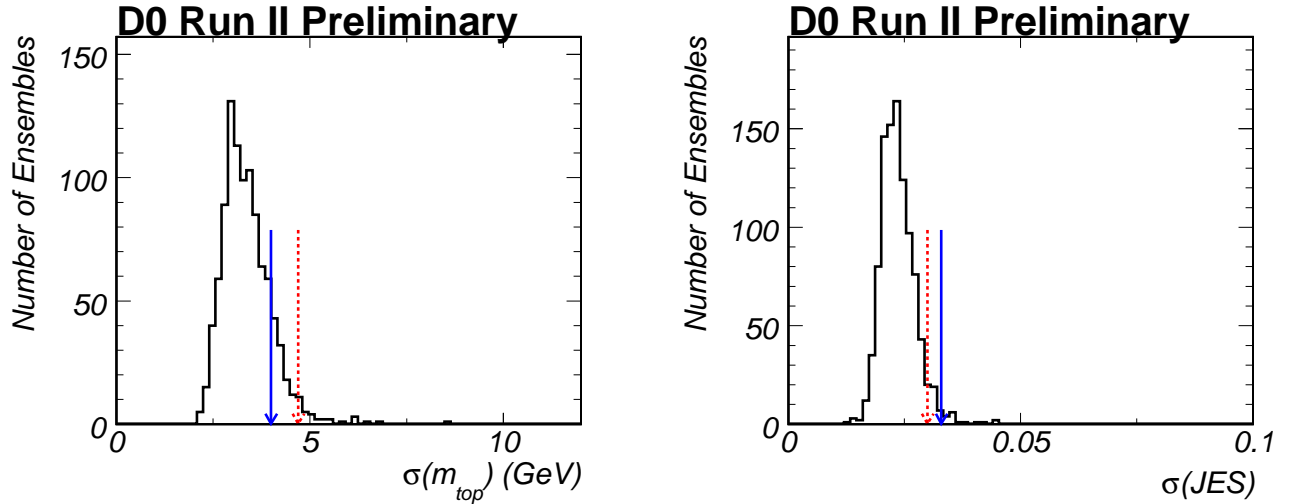


FIG. 10: Errors on m_{top} (left) and JES (right) obtained in the b tagging analysis with the combined sample. The distributions of fitted uncertainties obtained from ensemble tests are shown by the histograms. Both upper and lower uncertainties are shown; their distributions are very similar. The upper (lower) error in the data is indicated by the solid blue (dashed red) arrow.

- PDF uncertainty:** Leading-order matrix elements are used to calculate both P_{sgn} and P_{bkg} . Consequently, both calculations utilize a leading order parton distribution function (PDF): CTEQ5L [9]. To study the systematic uncertainty on m_{top} due to this choice, the variations provided with the next-to-leading-order PDF set CTEQ6M [10] are used, and the result obtained with each of these variations is compared with the result using the default CTEQ6M parametrization. The difference between the results obtained with the CTEQ5L and MRST leading order PDF sets is taken as another uncertainty. Finally, the effect of a variation of α_s is evaluated. In all cases, a large ensemble has been composed of events simulated with CTEQ5L, these have been reweighted such that distributions according to the desired PDF set are obtained, and the difference of results from the unweighted and weighted ensembles assigned as a systematic uncertainty. The individual systematic errors are added in quadrature.

- **b fragmentation:** While the overall jet energy scale uncertainty is included in the statistical uncertainty from the fit, differences in the b /light jet energy scale ratio between data and simulation may still affect the measurement. Possible effects from such differences are studied using simulated $t\bar{t}$ events with different fragmentation models for b jets. The default Bowler [11] scheme with $r_t = 1.0$ is replaced with $r_t = 0.69$ or with Peterson [12] fragmentation with $\epsilon_b = 0.00191$. One large ensemble is built using events from each of the three simulations. The absolute values of the deviations of top mass results from the standard sample are added in quadrature and symmetrized.
- **b/c semileptonic decays:** The reconstructed energy of b jets containing a semileptonic bottom or charm decay is in general lower than that of jets containing only hadronic decays. This can only be taken into account for jets in which a soft muon is reconstructed. Thus, the fitted top quark mass still depends on the semileptonic b and c decay branching ratios. They have been varied by reweighting events in one large ensemble of simulated events within the bounds given in [13].

B. Detector Modeling

- **JES p_T dependence:** The relative difference between the jet energy scales in data and Monte Carlo is fitted with a global scale factor, and the corresponding uncertainty is included in the quoted (stat. + JES) error. Any discrepancy between data and simulation other than a global scale difference may lead to an additional uncertainty on the top quark mass. To estimate this error, the energies of jets in the events of one large ensemble have been scaled by a factor of $(1 + 0.02 \frac{E_{\text{jet}}}{100 \text{ GeV}})$ where E_{jet} is the default jet energy. The value 0.02 is suggested by studies of γ +jets events. The top mass result from the modified ensemble has been compared to the default number, and the symmetrized difference is taken as systematic uncertainty.
- **Relative b /light jet energy scale:** Variations of the h/e calorimeter response lead to differences in the b /light jet energy scale ratio between data and simulation in addition to the variations of the b fragmentation function considered in Section VI A.
- **Trigger:** The trigger efficiencies used in composing ensembles for the calibration of the measurement are varied by their errors, and the uncertainties from all variations are summed in quadrature.
- **b tagging:** The b tagging efficiencies are varied within the uncertainties as determined from the data, and the variations are propagated to the final result.

Note that no systematic uncertainty is quoted due to multiple interactions/uranium noise as opposed to the Run I measurement. The effect is much smaller in Run II as a consequence of the reduced integration time in the calorimeter readout. It is moreover covered by the jet energy scale uncertainty, as the offset correction is computed separately for data and Monte Carlo in Run II, accounting for effects arising from electronic noise and pileup.

C. Method

- **Signal fraction:** The signal fraction f_{top} is slightly overestimated for low true signal fractions, which leads to a small bias in the resulting top mass. The signal fraction in ensemble tests used for the calibration is varied within the uncertainties determined from the topological likelihood fit, and the resulting variation of the top mass is taken as systematic uncertainty.
- **QCD background:** The W +jets simulation is used to model the small QCD background in the selected event sample in the analysis. The systematic uncertainty from this assumption is computed by selecting a dedicated QCD-enriched sample of events from data by inverting the lepton isolation cut in the event selection. The calibration of the method is repeated with ensembles formed where these events are used to model the QCD background events whose fraction is given in Table I.
- **MC calibration:** The calibration of the top mass measurement is varied according to the statistical uncertainty of the calibration curve shown in Figures 2 and 6.

VII. CONCLUSION

The matrix element technique has been extended to make use of b tagging information for the determination of the top quark mass. We apply the matrix element method to a 370 pb^{-1} data set recorded with the $D\bar{O}$ experiment at the Run II Tevatron and measure the top quark mass in lepton+jets $t\bar{t}$ events to be

$$m_{\text{top}}^{\ell+\text{jets}}(\text{topo}) = 169.2^{+5.0}_{-7.4}(\text{stat.} + \text{JES})^{+1.5}_{-1.4}(\text{syst.}) \text{ GeV} \text{ and}$$

$$m_{\text{top}}^{\ell+\text{jets}}(b\text{-tag}) = 170.6^{+4.0}_{-4.7}(\text{stat.} + \text{JES}) \pm 1.4(\text{syst.}) \text{ GeV} ,$$

where information about identified b jets is only used in the second result. The uncertainty on the jet energy scale is included in the statistical error, as the overall jet energy scale relative to the simulation is determined simultaneously with the top quark mass. We find values for the jet energy scale that indicate good consistency with the simulation.

Acknowledgments

We thank the staffs at Fermilab and collaborating institutions, and acknowledge support from the DOE and NSF (USA); CEA and CNRS/IN2P3 (France); FASI, Rosatom and RFBR (Russia); CAPES, CNPq, FAPERJ, FAPESP and FUNDUNESP (Brazil); DAE and DST (India); Colciencias (Colombia); CONACyT (Mexico); KRF (Korea); CONICET and UBACyT (Argentina); FOM (The Netherlands); PPARC (United Kingdom); MSMT (Czech Republic); CRC Program, CFI, NSERC and WestGrid Project (Canada); BMBF and DFG (Germany); SFI (Ireland); Research Corporation, Alexander von Humboldt Foundation, and the Marie Curie Program.

-
- [1] $D\bar{O}$ Collaboration, *Top Quark Mass Measurement with the Matrix Element Method in the Lepton+Jets Final State at $D\bar{O}$ Run II*, $D\bar{O}$ note 4874-CONF.
 - [2] $D\bar{O}$ Collaboration, V. Abazov *et al.*, *The Upgraded $D\bar{O}$ Detector*, submitted to Nucl. Instrum. Methods Phys. Res. A.
 - [3] $D\bar{O}$ Collaboration, S. Abachi *et al.*, Nucl. Instrum. Methods Phys. Res. A 338, 185 (1994).
 - [4] V.M. Abazov *et al.*, *The Muon System of the Run II $D\bar{O}$ Detector*, physics/0503151 (2005).
 - [5] V.M. Abazov *et al.* [$D\bar{O}$ Collaboration], *Measurement of the $t\bar{t}$ Production Cross Section in $p\bar{p}$ Collisions at $\sqrt{s} = 1.96$ TeV using Kinematic Characteristics of Lepton+Jets Events*, hep-ex/0504043 (2005).
 - [6] V. M. Abazov *et al.*, Phys. Lett. B **626**, 35 (2005).
 - [7] F.A. Berends, H. Kuijf, B. Tausk, W.T. Giele, *On the Production of a W and Jets at Hadron Colliders*, Nucl. Phys. B357:32-64 (1991).
 - [8] M.L. Mangano *et al.*, *ALPGEN, a Generator for Hard Multiparton Processes in Hadronic Collisions*, JHEP 307, 1 (2003).
 - [9] H. L. Lai *et al.* [CTEQ Collaboration], *Global QCD analysis of parton structure of the nucleon: CTEQ5 parton distributions*, Eur. Phys. J. C 12, 375 (2000).
 - [10] J. Pumplin *et al.*, *New Generation of Parton Distributions with Uncertainties from Global QCD Analysis*, JHEP 0207, 012 (2002).
 - [11] M.G. Bowler, *e^+e^- Production of Heavy Quarks in the String Model.*, Z. Phys C11, 169 (1981).
 - [12] C. Peterson *et. al.*, *Scaling Violations in Inclusive e^+e^- Annihilation Spectra*, Phys. Rev. D27, 105 (1983).
 - [13] The ALEPH, DELPHI, L3, OPAL, and SLD Collaborations, the LEP Electroweak Working Group, SLD Electroweak Group, and SLD Heavy Flavour Group, SLAC-R-774, (2005), hep-ex/0509008.